

# Supporting Information

For

## Photochemical-Induced Self-Seeding Effect on Lead Zirconate Titanate Thin Film

*Ching-Chich Leu\**, *Ching-Pin Hsu*, *Cin-Guan Hong* and *Chen-Ti Hu*

**Table S1** Light sources information.

	Wavelength	Company	Model and Specifications
<b>Halo</b>	>370nm	Dolan-Jenner Industries, Inc. (Lawrence, MA, USA)	Fiber-Lite DC950 illuminator: Lamp (EKE): 150W, 21V Quartz halogen(with the fiber optic connected to the illuminator)
<b>UVA</b>	365 nm	UVP, LLC (Upland, CA, USA)	Mineralight Display Lamp (UVL-225D): Two 25-watt UV(365nm) tubes
<b>UVC</b>	254 nm	UVP, LLC (Upland, CA, USA)	R-52 Grid Lamp (R-52G): A high intensity 254nm UV grid, 1250 $\mu$ W/cm <sup>2</sup> at 6 inches with the filter

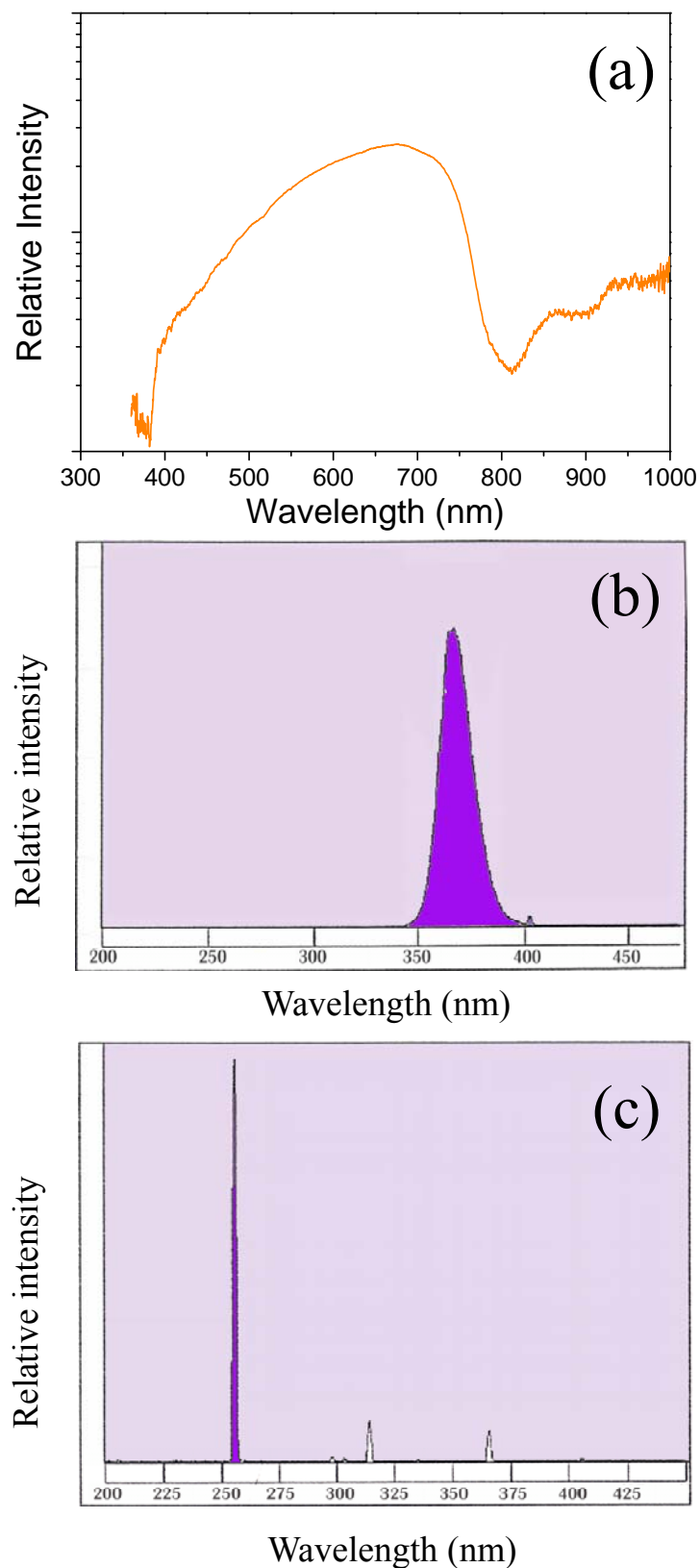


**Figure S1** The intensity spectra of (a) quartz halogen light, (b) 365 nm-UV light, and (c) 254 nm-UV light. UV lamp with emission centered at a wavelength of 254 nm and 365nm.

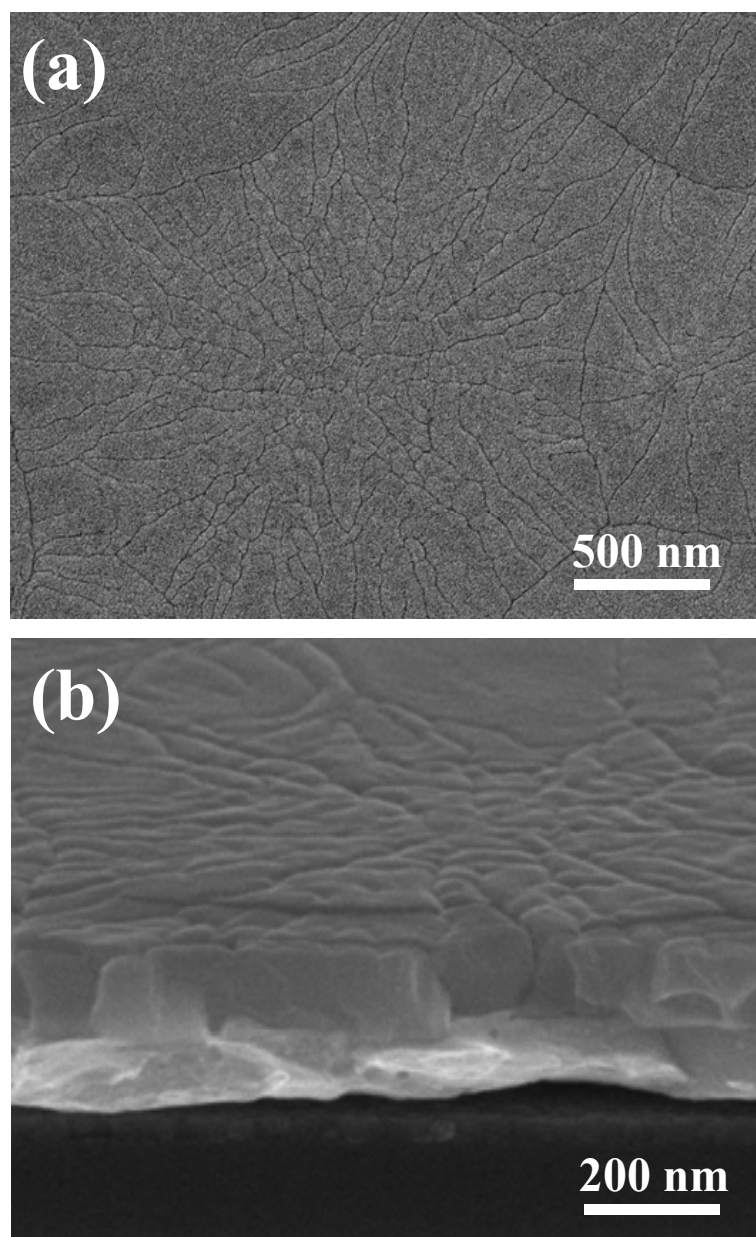


**Figure S2** The SEM (a) surface, and (b) tilted images of the UVC-Z60. It is clearly observed that these rosettes are aggregates of nano-sized columnar grains.

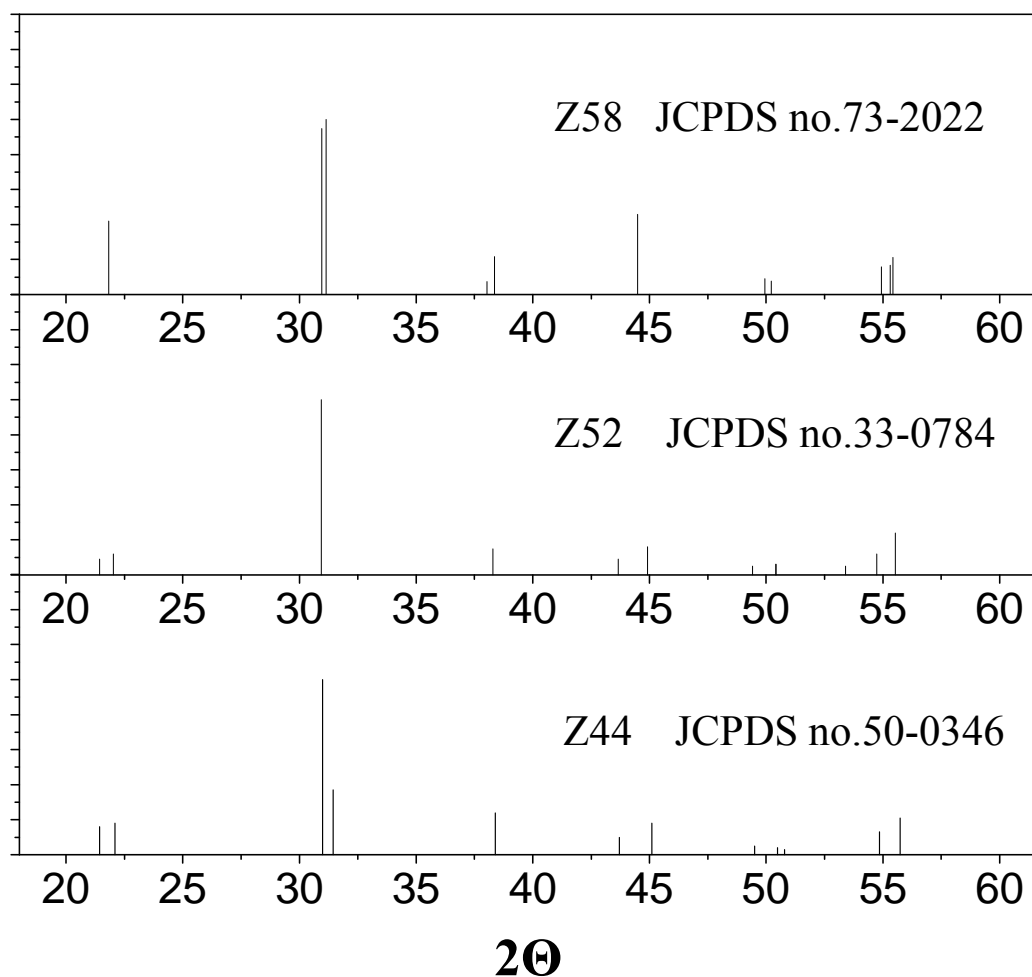


**Figure S3** The JCPDS database of the PZT whose compositions are near the Z60, Z52 and Z40.

## ***Visualization of the domain configuration of PZT:***

To investigate the local distribution of the remanent polarization in a PZT film, piezoresponse force microscopy (PFM) was employed.<sup>1</sup> The experiment was performed under ambient conditions by using a commercial AFM (Solver PRO-M, NT-MDT). To apply an external electric field in the sample, we used a Cr/Pt-coated silicon cantilever (ElectriCont-G, Budgetsensors) with a spring force constant lying between 0.07~0.4 Nm<sup>-1</sup> and an integrated tip radius less than 25 nm. In this study, PZT films were imaged by superimposing a small AC voltage of 1 V in amplitude and of 170 kHz in frequency between the tip and the Pt bottom electrode of a PZT film. The phase-sensitive vertical deflection of the cantilever caused by the converse piezoelectric effect was sent to a lock-in amplifier and recorded as the piezoresponse image simultaneously with the topographic image. Consequently, a high-contrast region in a PFM image indicated a ferroelectric domain with its remanent polarization pointing up or down. On the other hand, a domain with its polarization parallel to the film showed a less-contrast image.

Figures S4a and S4b show the morphology image and its corresponding piezoresponse pattern of the Ref- Z60 within a area of 5× 5μm<sup>2</sup>, respectively. Three contrast states, i.e., white, black and gray, are clearly observed within the micrograins in the piezoresponse image. White and black regions correspond to the positive (polarization upward) and the negative ferroelectric domain, respectively; so these two contrasting images represent two anti-parallel out-of-plane domains.<sup>2</sup> The gray regions, without a net black or white contrast, correspond to areas of the sample that possess a very weak piezoelectric activity. To demonstrate the switching properties of the Ref- Z60, a domain pattern was artificially prepared on this film. First, a relatively large square area of 5μm × 5μm was polarized by scanning with a positive 10V applied onto the tip; next, a central square 2.5μm × 2.5μm domain pattern was written under a negative 10V. The applied voltage of 10V is high enough to switch the polarization of the domain. After being written, the AFM and the piezoresponse image were again acquired, as shown in Figures S5a and S5b. Figure S5b clearly depicts a generated pattern, suggesting most areas are effectively switched up or down; but, there exists some un-switched regions within the pattern. It is noting that most un-switched regions are corresponding to the gray regions which have already been there before switching. These gray regions are mainly associated with the small grain regions, the grain boundaries, or randomly oriented grains in polycrystalline structures. Nano-scale grains and grain boundaries possess less crystallinity and are more difficult to switch in polarity, as compared to the large grains. The domains where the polarization deviates from the normal direction of the film's plane are relatively difficult to switch, as proposed by A. Gruveman.<sup>2</sup> Therefore, such weak contrast regions might contribute little to the macroscopic polarization value.

The UVA- and the Halo- Z60 exhibited nearly the same textures and grain structures as the Ref- Z60; they also own the similar domain structures and switching characteristics. (not shown here) In contrast, the domain structure, corresponds to the rosette structure, of the UVC- Z60 is quite different with that in the Ref- Z60, as indicated in Figure S4c and S4d. The particular domain configuration in the UVC- Z60 is possible due to the specific grain structure of the rosette. An artificially generated domain patterns is also prepared in this specimen (Figure S5c and S5d). Although the rosettes are composed of numerous tiny grains, their most domains could be effectively switched by applied 10V. Domain visualization was also conducted on the Z52 or the Z40 (not shown here); their granular structures showed similar domain configuration to that of the Ref- Z60 regardless of photo-assisted conditions.

## Reference

1. Gruverman, A.; Auciello, O.; Tokumoto, H. *Ann. Rev. Mater. Sci.*, **1998**, *28*, 101.
2. Gruverman, A.; Ikeda, Y. *Jpn. J. Appl. Phys.*, **1998**, *37*, L939.



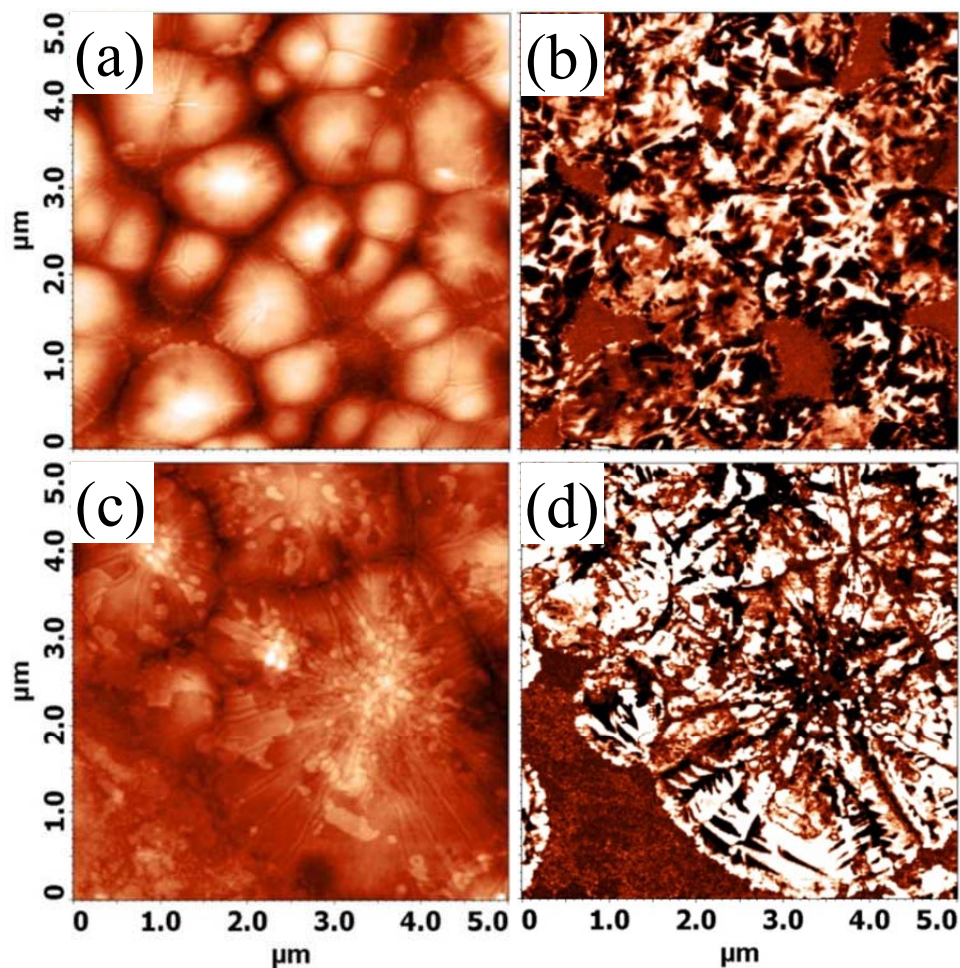


**Figure S4** The AFM and the corresponding PFM images of Ref-Z60 ((a) and (b)), and UVC-Z60 ((c) and (d)), respectively.

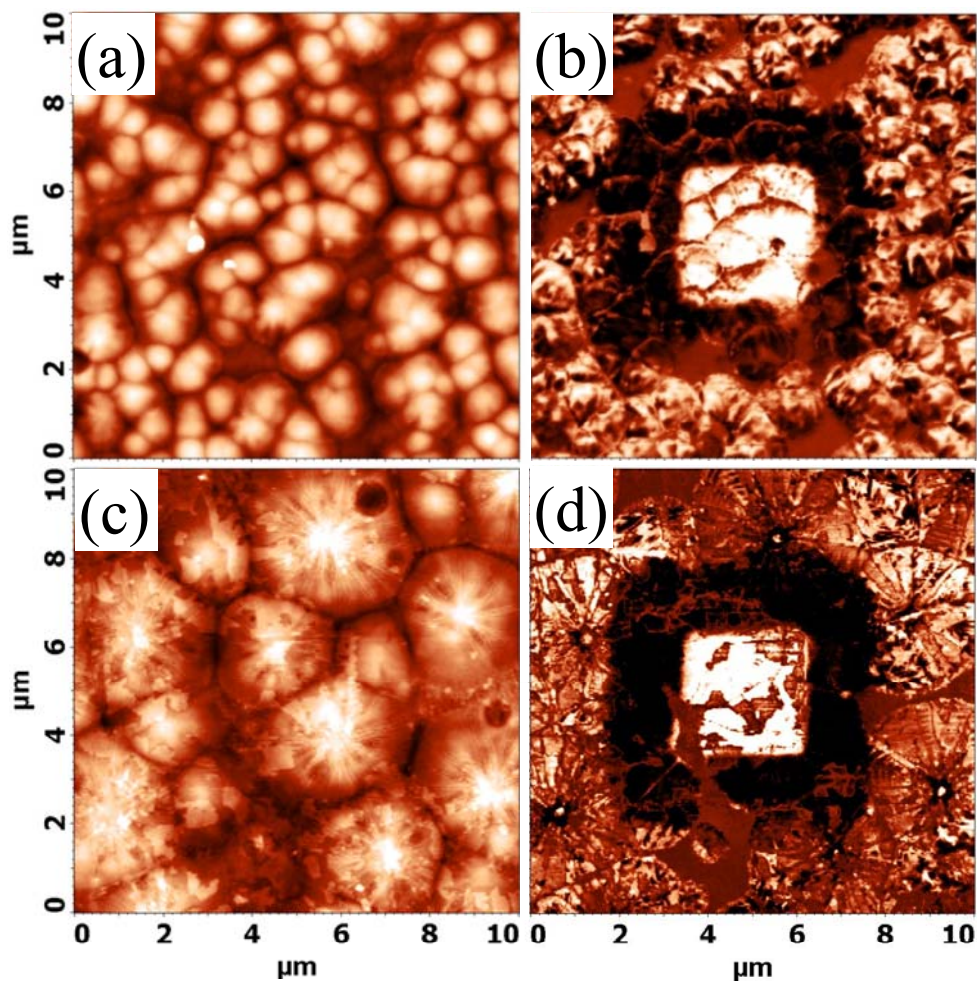


**Figure S5** The AFM and the corresponding PFM images of Ref-Z60 ((a) and (b)), and UVC-Z60 ((c) and (d)), respectively. An artificially generated domain pattern is prepared by scanning these specimens with 10V/-10V.



## ***Calculation of the contributed polarization from polarization axes of PZT:***

To correlate the variations of remanent polarization values to their texture structure of PZT, calculation of the contributed polarization from various polarization axes was performed. Funakubo *et al.* reported that the constitution phase (mainly, rhombohedral and tetragonal phases) of PZT films were dependent on the Zr/(Zr+Ti) ratio in the film.<sup>1</sup> And, Noheda *et al.* have proved the existence of monoclinic phase in between the previously established tetragonal and rhombohedral regions.<sup>2</sup> This monoclinic structure was demonstrated to bridge between the well-known tetragonal and rhombohedral phases in the PZT phase diagram where the morphotropic phase boundary (MPB) was delimited. Therefore, in this case, the Z40 and the Z60 exhibited the rhombohedral and the tetragonal structure, respectively, while the Z52 could be ascribed to the monoclinic phase. The polar axes are the [111] and [001] axes for ferroelectric compositions with rhombohedral and tetragonal symmetry,<sup>3</sup> respectively, on either side of the MPB and the polar axis in the monoclinic phase is found to be tilted about 24° from the [001] axis towards the [111] axis.<sup>4</sup> The contributed polarization values of each plane was obtained by multiplying the Pr values with their integrated intensity ratio ( $Pr_{(hkl)} \times \alpha_{(hkl)}$ ).  $\alpha_{(hkl)}$  is the integrated intensity ratio of each peak, which is defined as

$$\alpha_{(hkl)} = \frac{I_{(hkl)}}{I_{(100)} + I_{(001)} + I_{(110)} + I_{(101)} + I_{(111)}}$$

, where  $I_{(100)}$  represents the peak area of (100) peak, and vice versa. We used a software to deconvolute the overlapped diffraction peaks and integrated their peak area individually.

For example: the spontaneous polarization direction in tetragonal structure is along the c-axis, there is no polarization contribution from either (100) or (110) planes due to their normal vectors were perpendicular to [001]. Additionally, the tilted angles between (101) and (001) was 45.81°, and was 55.49° between (111) and (001), therefore the Pr values of these two planes are  $Pr_{(101)} = Pr_{(001)} \times \cos 45.81^\circ$  and  $Pr_{(111)} = Pr_{(001)} \times \cos 55.49^\circ$ . Then, the contributed polarization values normal to the film surface is a summation of all the calculated polarization values of each plane. Figure S6b shows the calculated polarization values as functions of light-exposure conditions for the Z60, the Z52, and the Zr40. Noting that all the calculated polarization values are normalized by those of their polar axes.

### **Reference**

1. Funakubo, H.; Tokita, K.; Oikawa, T.; Aratani, M.; Saito, K. *J. Appl. Phys.*, **2002**, *92*, 5448.
2. Noheda, B.; Cox, D. E.; Shirane, G.; Gonzalo, J. A.; Cross, L. E.; Park, S. E. *Appl. Phys. Lett.*, **1999**, *74*, 2059.
3. Gong, W.; Li, J. F.; Li, L. *J. Appl. Phys.*, **2004**, *96* (1), 590.
4. Noheda, B.; Gonzalo, J. A.; Cross, L. E.; Guo, R.; Park, S. E.; Cox, D. E.; Shirane, G. *Phys. Rev. B.*, **2000**, *61*, 8687.

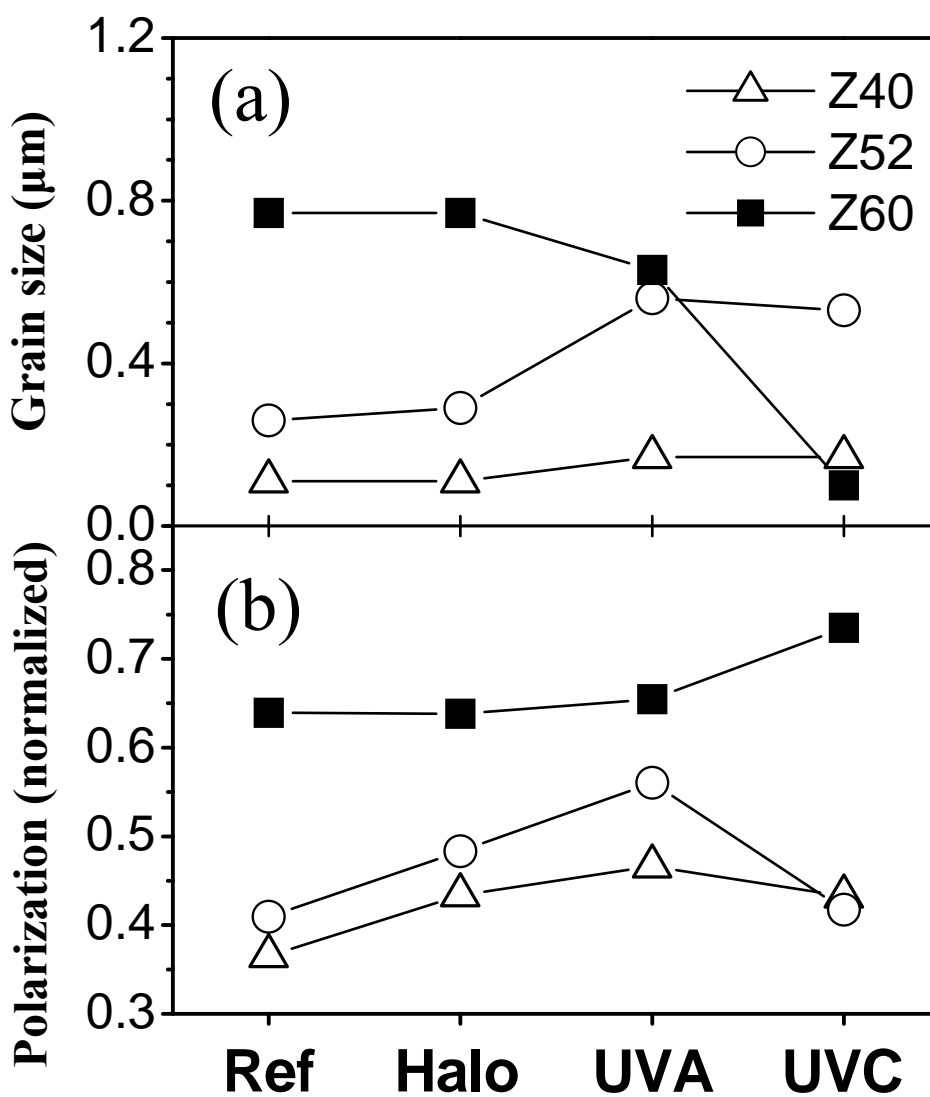


**Figure S6** (a) the variations of grain sizes as functions of light-exposure conditions for Z60, Z52, and Zr40. (b) the calculated polarization values normal to film surface as functions of light-exposure conditions for Z60, Z52, and Zr40. All the calculated polarization values are normalized by those of their polar axes.

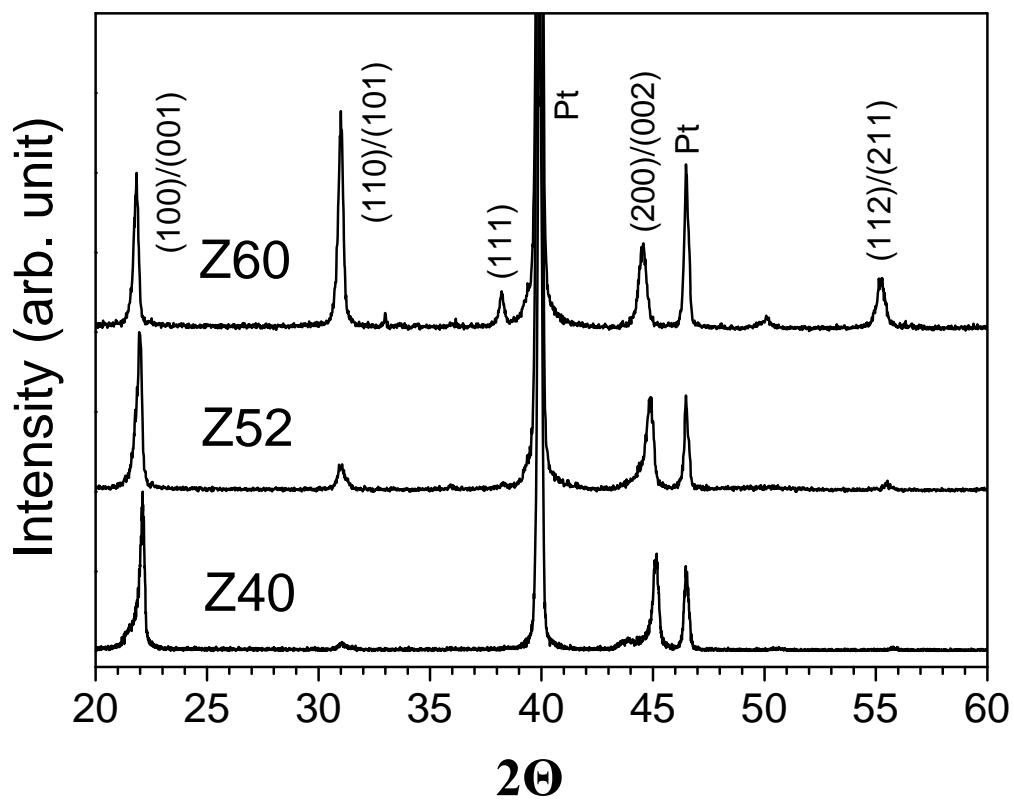


**Figure S7** The XRD patterns of the reference specimens of the PZT with a 5 mole % excess of PbO.

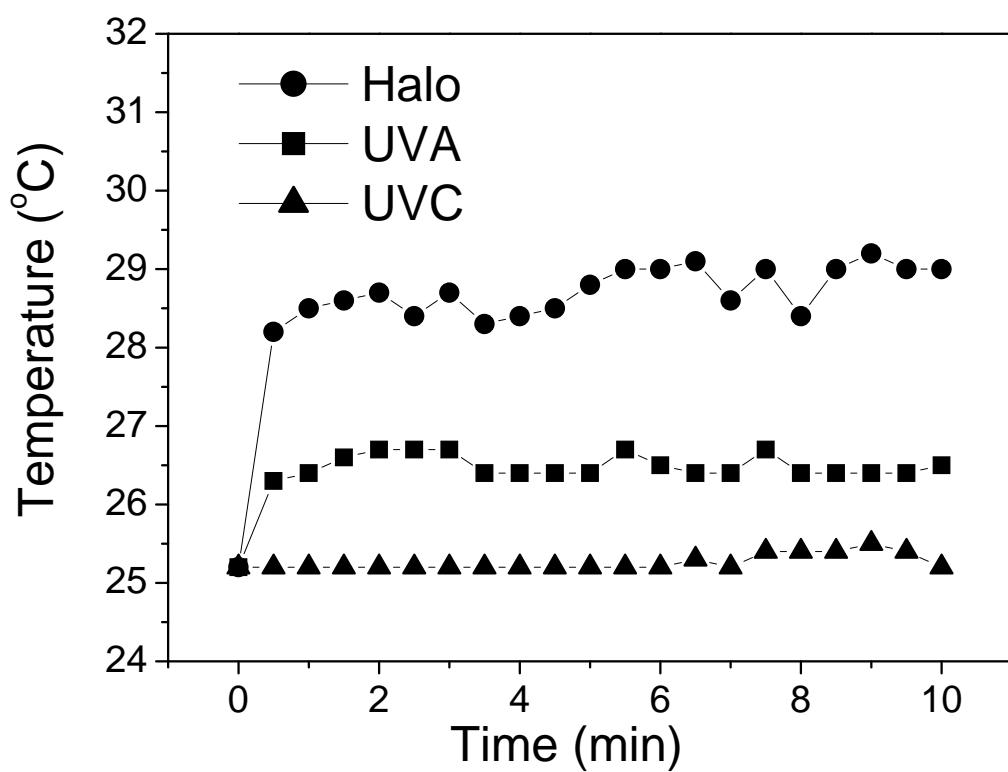


**Figure S8** The variation in the sample surface temperature during halogen-light the Halo- light, the UVA- light, and the UVC- light exposure.